Electronic Supplementary Material (ESI) for Physical Chemistry Chemical Physics.

Supplementary Information

Membrane packing defects in synaptic vesicles recruit complexin and synuclein

Jie Liu, Bing Bu, Michael Crowe, Dechang Li, Jiajie Diao, Baohua Ji

1. Supporting tables
2. Supporting figures
3. References

1. Supporting tables

Table S1. MD simulations for defect analysis.

Diameter of the membranes (nm)	Lipid components	Conformations	Simulation time (ns)
∞	DOPC: DOPS (88%: 12%)	Flat	100
	DOPC: DOPS: CHOL (68%: 12%: 20%)	Flat	100
	DOPC: DOPS: CHOL (38%: 12%: 50%)	Flat	100
	DOPC: DOPS: DOPE (68%: 12%: 20%)	Flat	100
	DOPC: DOPS: DOPE (38%: 12%: 50%)	Flat	100
24	DOPC: DOPS (88%: 12%)	Cap	100
	DOPC: DOPS: CHOL (68%: 12%: 20%)	Cap	100
	DOPC: DOPS: CHOL (38%: 12%: 50%)	Cap	100
	DOPC: DOPS: DOPE (68%: 12%: 20%)	Cap	100
	DOPC: DOPS: DOPE (38%: 12%: 50%)	Cap	100
	DOPC: DOPS (88%: 12%)	Vesicle	100
	DOPC: DOPS: CHOL (38%: 12%: 50%)	Vesicle	100
54	DOPC: DOPS (88%: 12%)	Cap	100
	DOPC: DOPS: CHOL (68%: 12%: 20%)	Cap	100
	DOPC: DOPS: CHOL (38%: 12%: 50%)	Cap	100
	DOPC: DOPS: DOPE (68%: 12%: 20%)	Cap	100
	DOPC: DOPS: DOPE (38%: 12%: 50%)	Cap	100

Table S2. MD simulations of protein binding to membranes with varied curvatures.

Diameter of the membrane (nm)	Protein	Lipid components	Initial state of protein	Simulation time (ns)	Independent simulations
∞	CTD	DOPC: DOPS (88%: 12%)	Horizontal	100	5
	CTD	DOPC: DOPS: CHOL (38%: 12%: 50%)	Horizontal	100	5
	CTD	DOPC: DOPS: DOPE (38%: 12%: 50%)	Horizontal	100	5
	CTD	DOPC: DOPS (88%: 12%)	Vertical	100	3
	CTD	DOPC: DOPS: CHOL (38%: 12%: 50%)	Vertical	100	3
	CTD	DOPC: DOPS: DOPE (38%: 12%: 50%)	Vertical	100	3
	NTD	DOPC: DOPS (88%: 12%)	Horizontal	100	5
	NTD	DOPC: DOPS: CHOL (38%: 12%: 50%)	Horizontal	100	5
	NTD	DOPC: DOPS: DOPE (38%: 12%: 50%)	Horizontal	100	5
	NTD	DOPC: DOPS (88%: 12%)	Vertical	100	3
	NTD	DOPC: DOPS: CHOL (38%: 12%: 50%)	Vertical	100	3
	NTD	DOPC: DOPS: DOPE (38%: 12%: 50%)	Vertical	100	3
24	CTD	DOPC: DOPS (88%: 12%)	Horizontal	100	5
	CTD	DOPC: DOPS: CHOL (38%: 12%: 50%)	Horizontal	100	5
	CTD	DOPC: DOPS: DOPE (38%: 12%: 50%)	Horizontal	100	5
	CTD	DOPC: DOPS (88%: 12%)	Vertical	100	3
	CTD	DOPC: DOPS: CHOL (38%: 12%: 50%)	Vertical	100	3
	CTD	DOPC: DOPS: DOPE (38%: 12%: 50%)	Vertical	100	3
	NTD	DOPC: DOPS (88%: 12%)	Horizontal	100	5
	NTD	DOPC: DOPS: CHOL (38%: 12%: 50%)	Horizontal	100	5
	NTD	DOPC: DOPS: DOPE (38%: 12%: 50%)	Horizontal	100	5
	NTD	DOPC: DOPS (88%: 12%)	Vertical	100	3
	NTD	DOPC: DOPS: CHOL (38%: 12%: 50%)	Vertical	100	3
	NTD	DOPC: DOPS: DOPE (38%: 12%: 50%)	Vertical	100	3

2. Supporting figures

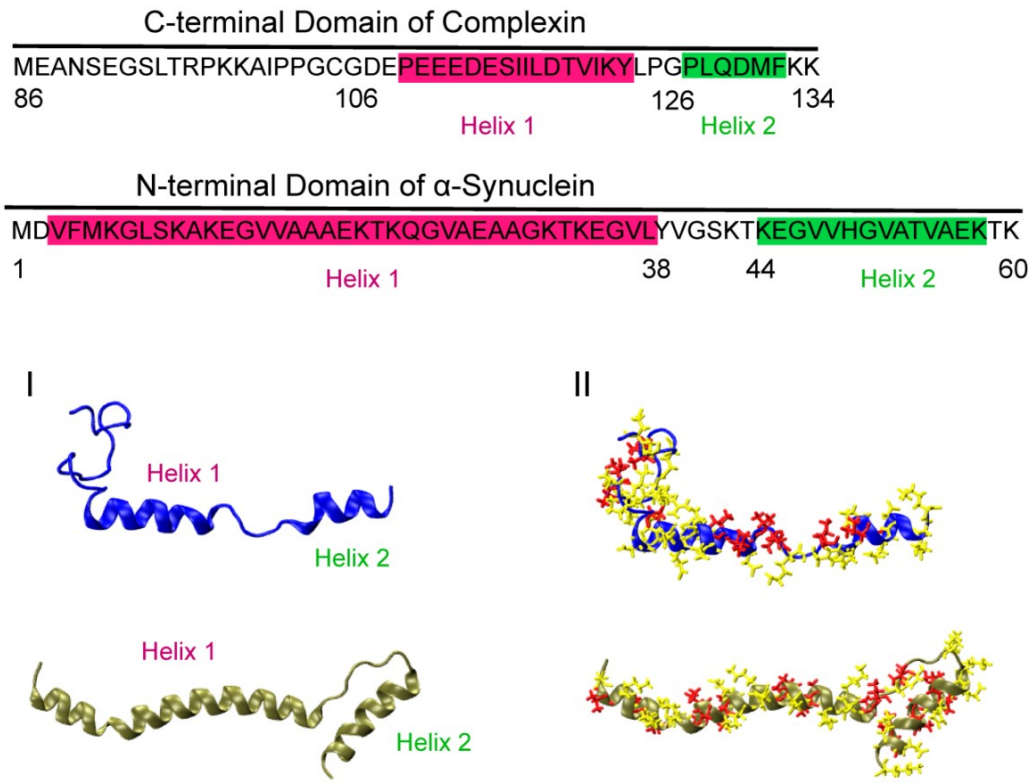

Figure S1. Sequences and structures of the CTD of Cpx and the NTD of α-Syn. Structures of the CTD and NTD were shown in the bottom insets I and II, respectively. The CTD structure of Cpx (i.e., residues 86 to 134) was generated according to the structural prediction from its sequence [1, 2]. The NTD structure of α-Syn (i.e., residues 1 to 60) was obtained from the Protein Data Bank with ID 1XQ8 [3]. In the insets II, the hydrophobic residues were shown explicitly by yellow rods, while the hydrophilic ones were shown in red color.

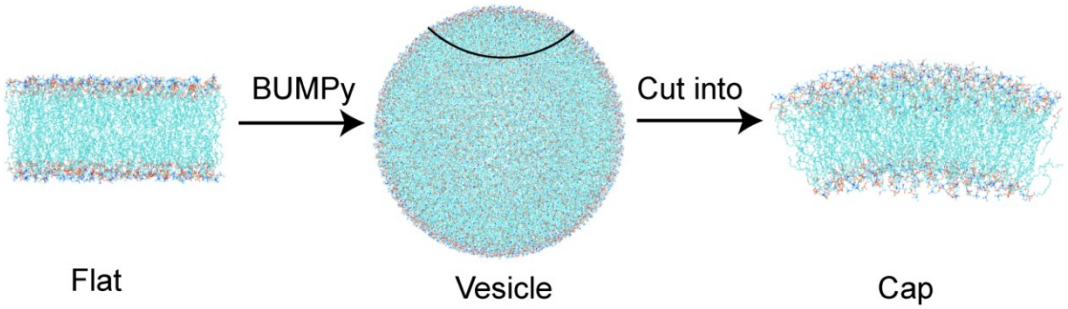

Figure S2. The setup of cap models of curved membrane. Flat membranes with targeted lipid component were built by the CHARMM-GUI [4]. Flat membranes were translated to a vesicle with varied diameters, i.e., D = 54 nm and D = 24 nm in this study, with BUMPy package [5]. A cap was cut out from the vesicle and used as the curved membrane model in this study.

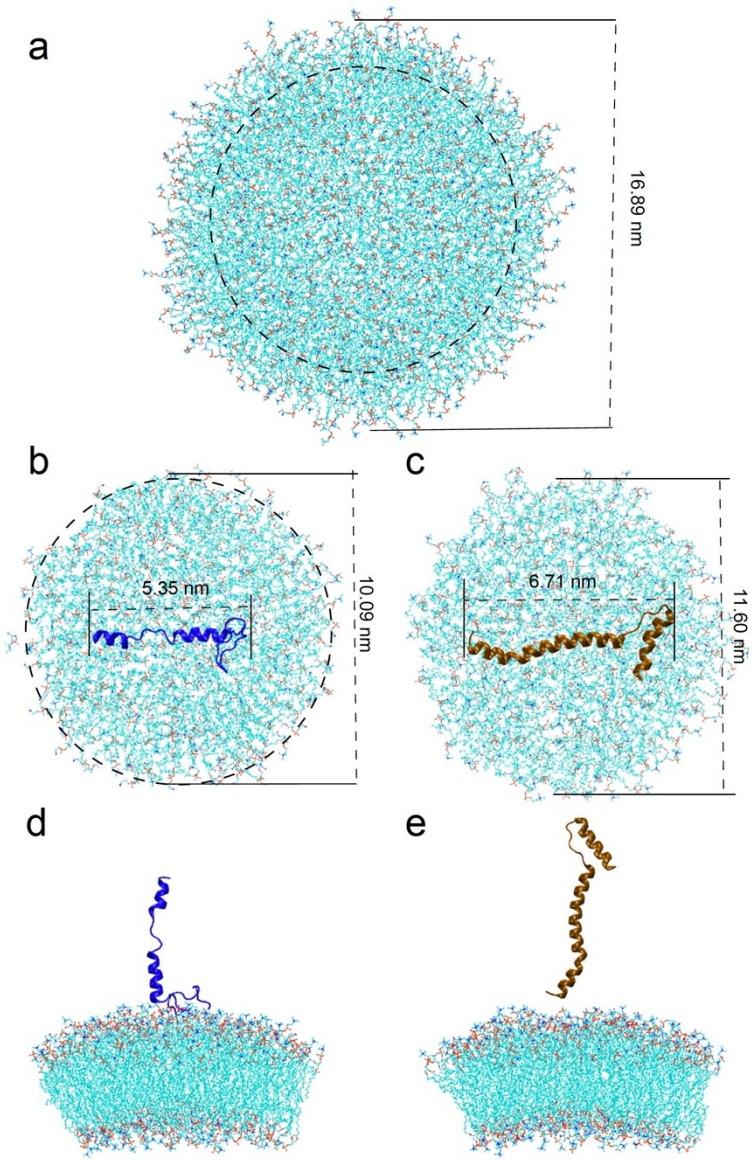

Figure S3. Illustration of the size of spherical caps in simulations. (a) The top view of the spherical cap used for defect analysis. (b) and (c) show the comparison of the size of Cpx's CTD and α-Syn's NTD with spherical caps used in protein binding simulations, respectively. (b) and (c) also show the initial structures of protein binding simulations with protein aligned horizontally to the membrane surface. (d) and (e) show the initial structures of protein binding simulations with the protein aligned vertically to the membrane surface. The circle in dash line in (a) and (b) indicates the size of caps. Blue color is the CTD of Cpx, while the NTD of α-Syn is orange.

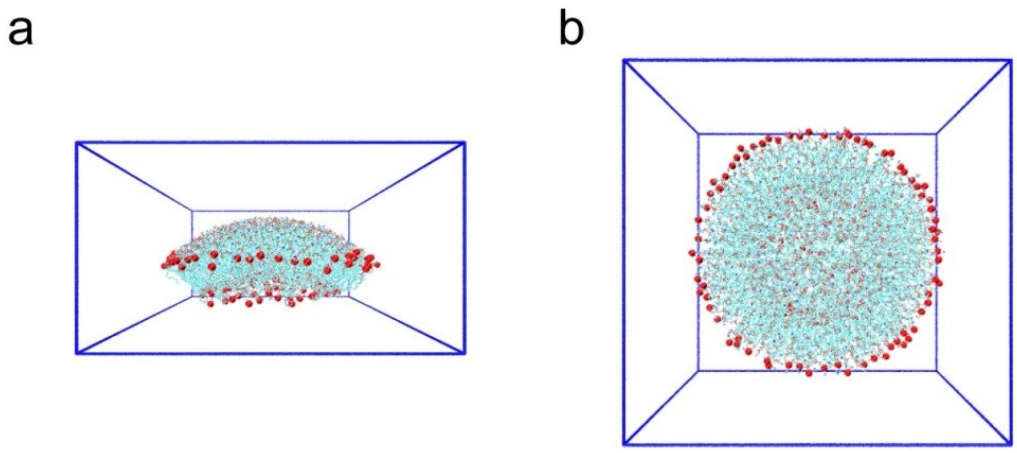

Figure S4. Illustration of the treatment of the cap model of the curved membrane in the simulation box with periodic boundary condition. (a) side and (b) top view of the cap in the simulation box. The lines in blue represent the boundary of the simulation box. Red dots are the restrained phosphorus atoms at the edge and the inner leaflet of the cap.

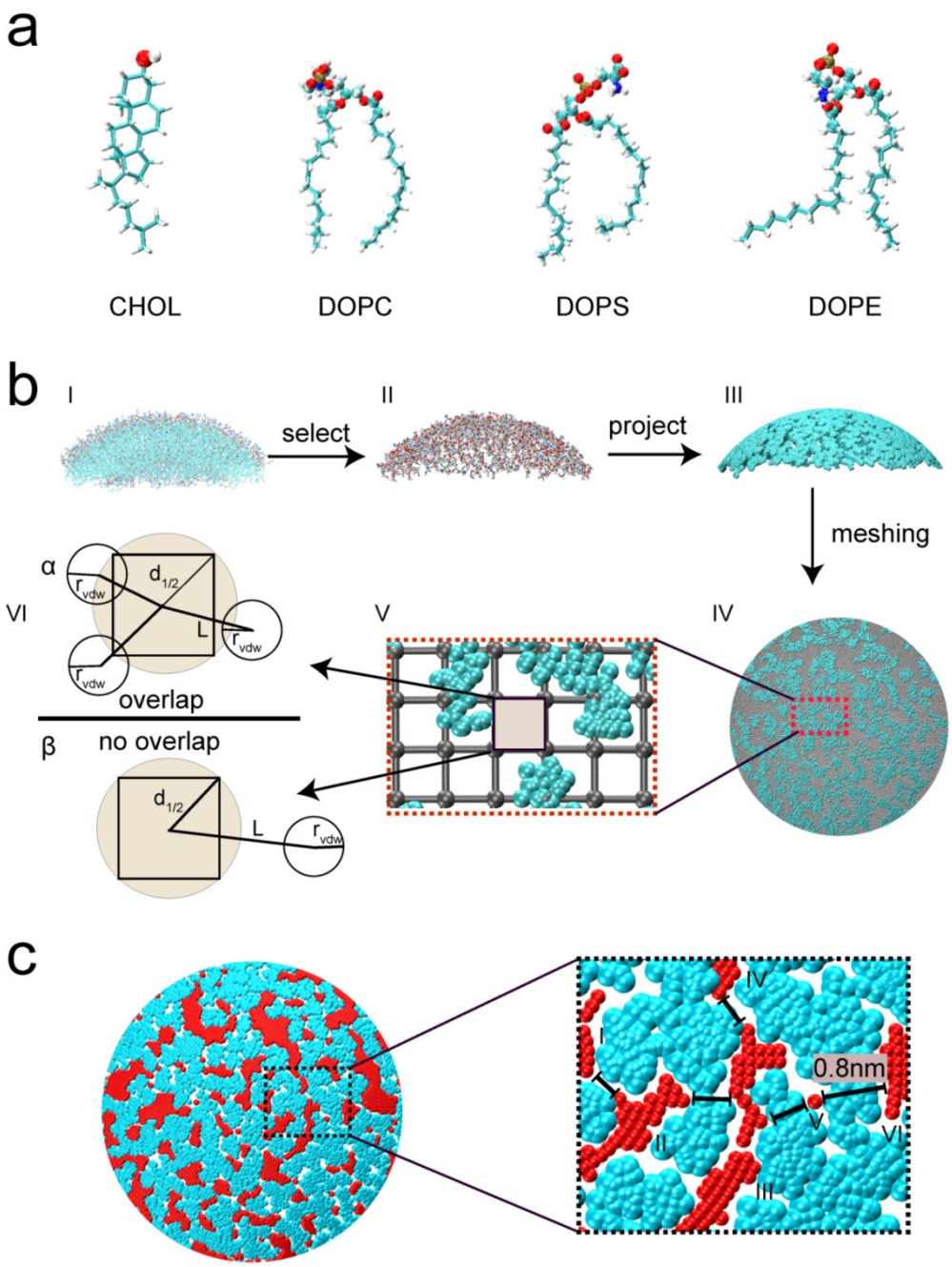

Figure S5. Analysis of defects in a curved membrane. (a) Illustrations of the structures of lipids CHOL, DOPC, DOPS, and DOPE. (b) The detection method of defects in curved membrane. Firstly, we selected the hydrophilic head groups of lipids and projected the head group atoms onto a spherical surface with corresponding curvatures (insets I to III). Next, a grid was meshed on the spherical surface with a grid size of 0.1 nm, as shown by the gray mesh in the inset IV and V. For each grid, we calculated

the distance *L* between the center of the grid and the mass center of the projected atom (VI). An overlap of the grid and the projected atom is assigned when *L* is shorter than the critical distance $d_c = r_{vdw} + d_{1/2}$, where r_{vdw} is the van der Waals radius of corresponding atoms and $d_{1/2} = 0.07$ nm is the half diagonal length of the grid (see the α state in VI). Otherwise, there is no overlap between the grid and the projected atom. Following the above method, if there is no overlap between a grid and any atoms, the grid is identified as a defect grid with the area of 0.01 nm^2. The defect grids within distance 0.3 nm are identified as in the same defect. The area of one defect thus defined as the total area of its defect grids. (c) The calculation of number of defects. According to previous work by Vamparys et al.[6], we identified the defect grids belong to two different defects when the two regions are not connected with a distance larger than 0.3 nm. For example, there are six defects in the zoom-in region in (c).

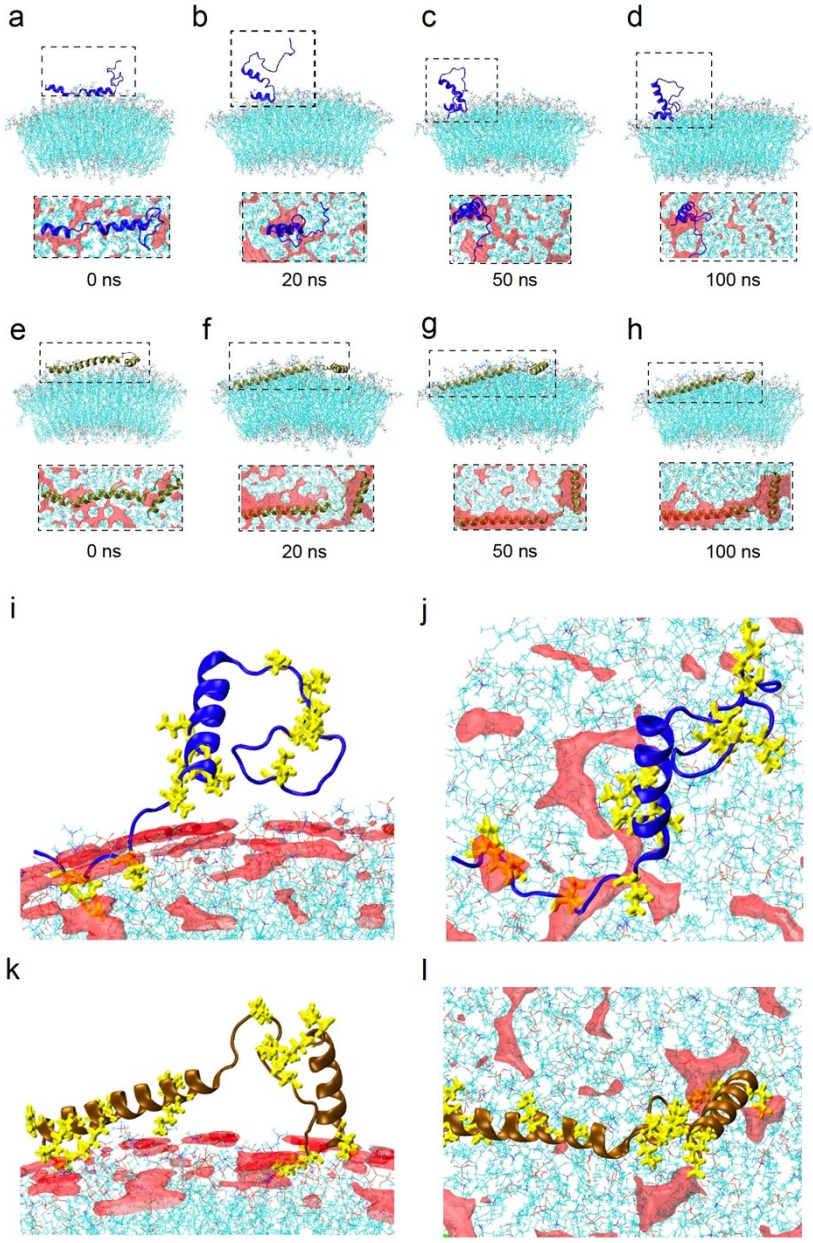

Figure S6. The binding process of the CTD (Cpx) and NTD (α-Syn) to membrane with a large defect area fraction. The snapshots of (a) to (d) CTD and (e) to (h) NTD binding to membrane, respectively, showing that the binding was associated with the insertion of the hydrophobic residues to membrane defects. (i) to (l) show more structural details of the insertion of the hydrophobic residues to packing defects. In (i) to (l), the hydrophobic residues are shown by yellow color, while defects in membrane are shown by the red color.

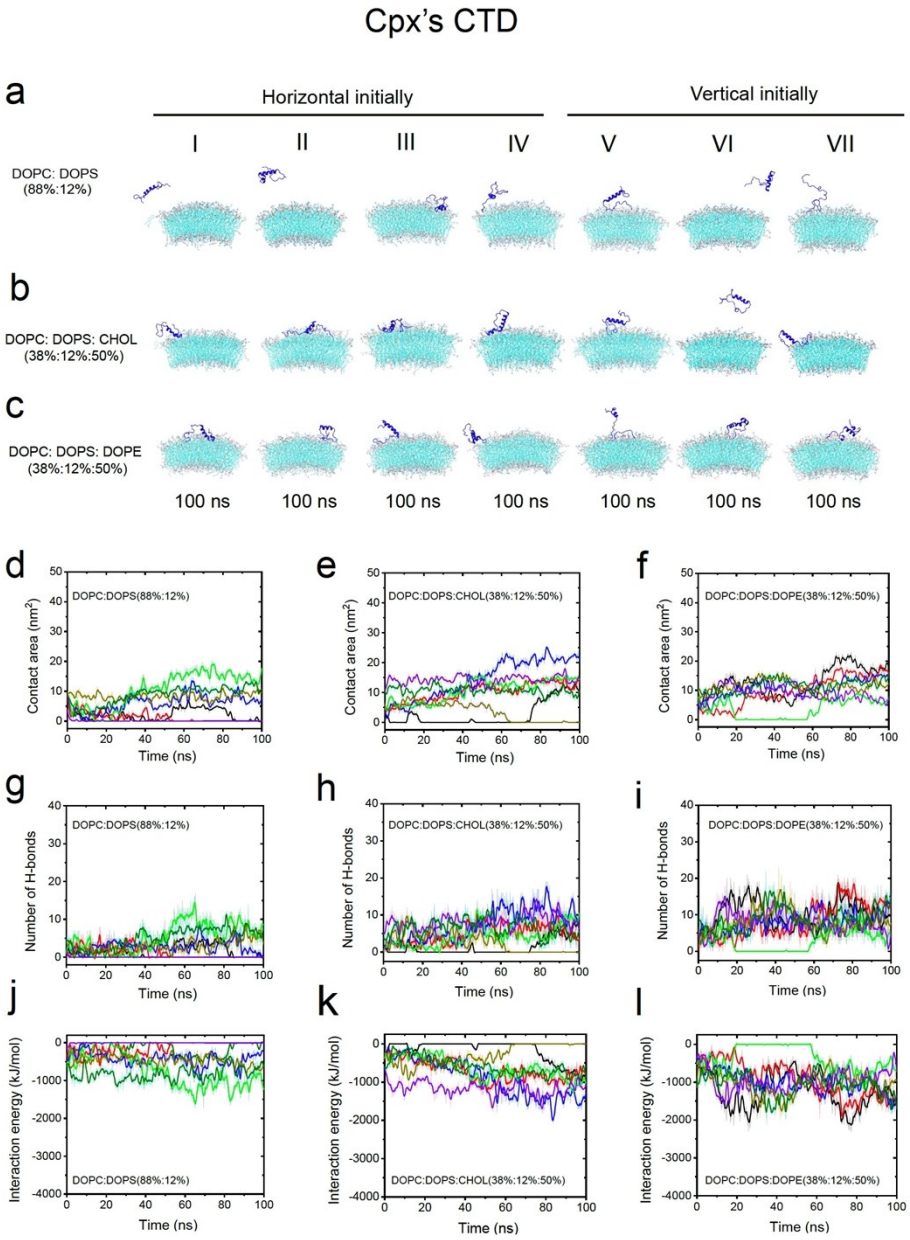

Figure S7. Additional seven simulation results of CTD binding to curved membranes with 24 nm diameter. (a), (b), and (c) Final states of the 100 ns simulations of CTD binding to membranes with varied lipid components. The roman numerals I, II, III, IV, V, VI, and VII labelled seven additional independent simulations. (d) to (f), (g) to (i), and (j) to (l) showed the contact area, the number of H-bonds, and the interaction energy of corresponding simulations, respectively. Each line in (d) to (l) by individual color represents the result of one of the independent simulations.

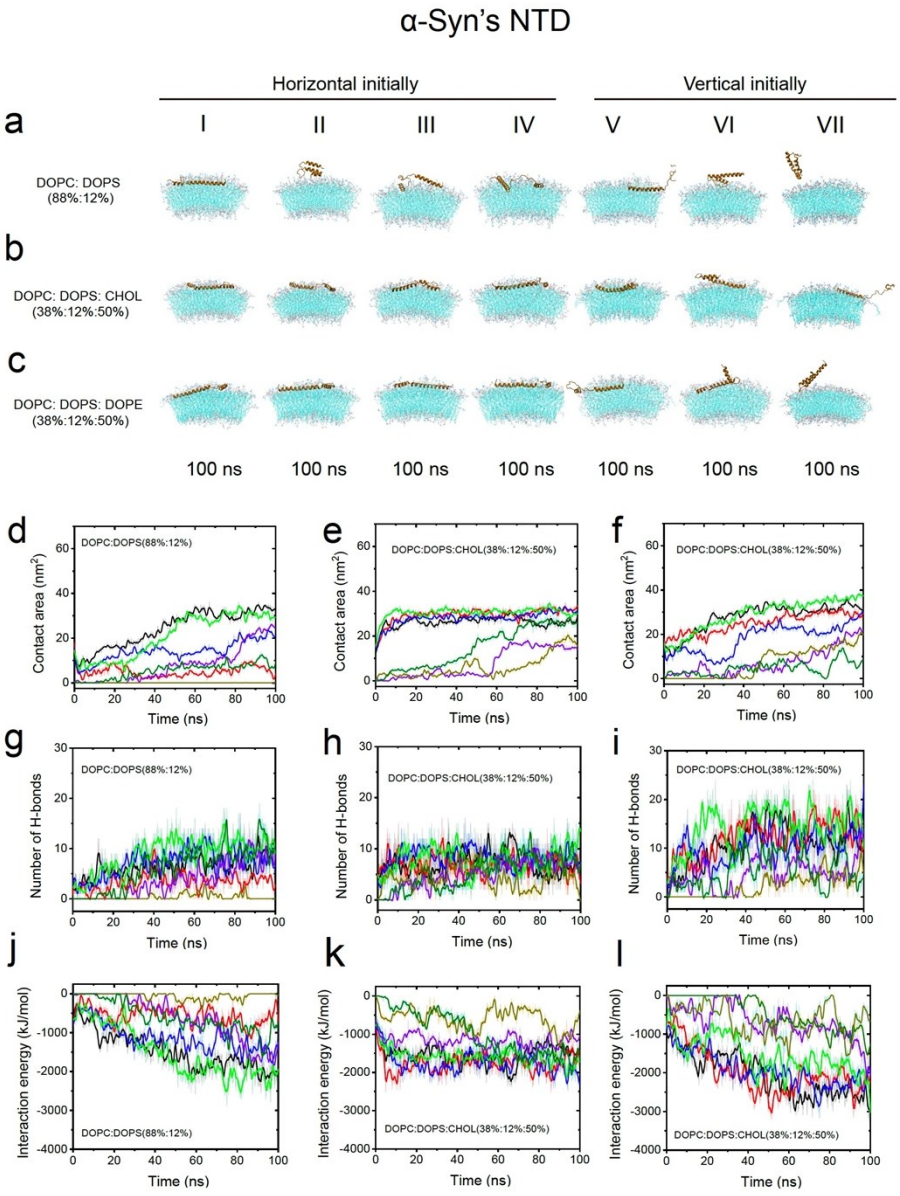

Figure S8. Additional seven simulation results of NTD binding to curved membranes with 24 nm diameter. (a), (b), and (c) Final states of the 100 ns simulations of NTD binding to membranes with varied lipid components. The roman numerals I, II, III, IV, V, VI, and VII labelled the seven additional independent simulations. (d) to (f), (g) to (i), and (j) to (l) show the contact area, the number of H-bonds, and the interaction energy of corresponding simulations, respectively. Each line in (d) to (l) by individual color represents the result of one of the independent simulations.

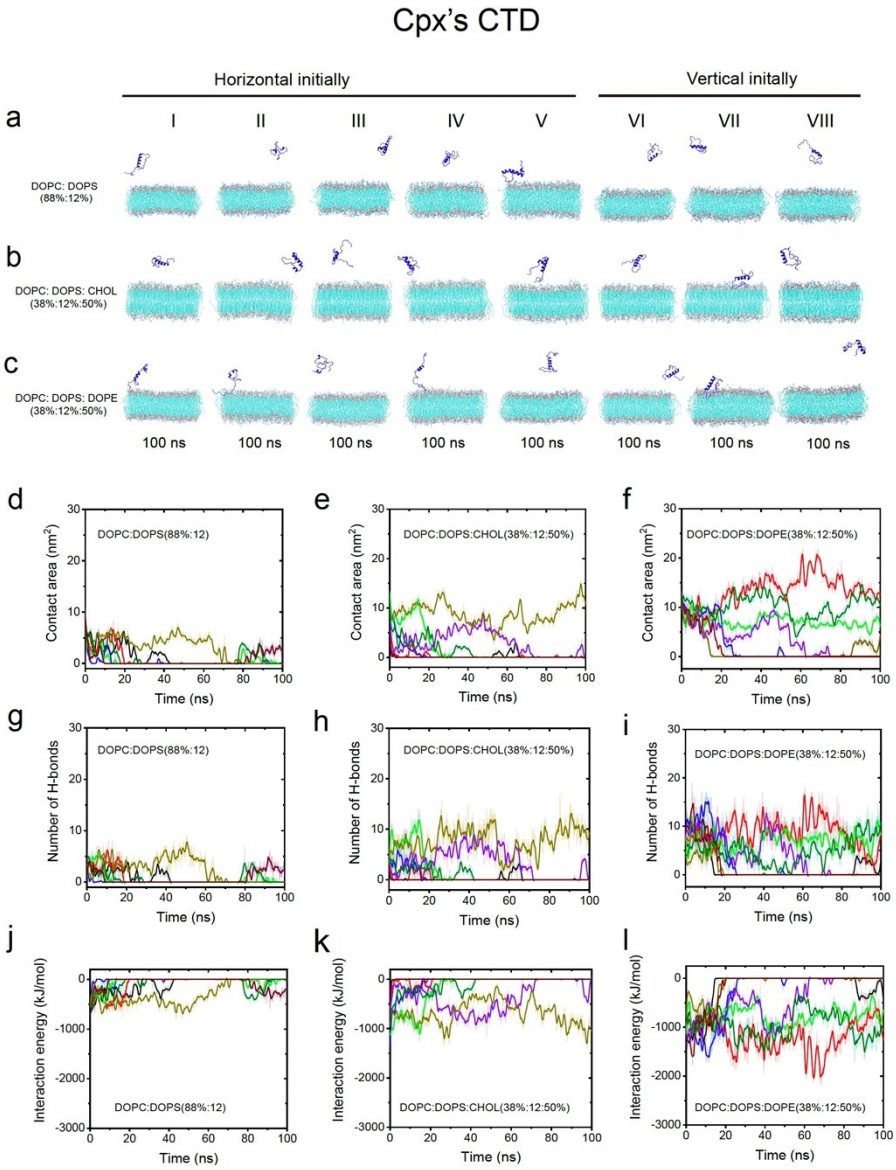

Figure S9. Eight independent simulations of the Cpx's CTD binding to a flat membrane. (a), (b), and (c) Final states of the 100 ns simulations of CTD binding to membranes with varied lipid components. The roman numerals I, II, III, IV, V, VI, VII, and VIII labelled the eight independent simulations. (d) to (f), (g) to (i), and (j) to (l) show the contact area, the number of H-bonds, and the interaction energy of corresponding simulations, respectively. Each line in (d) to (l) by individual color represents the result of one of the independent simulations.

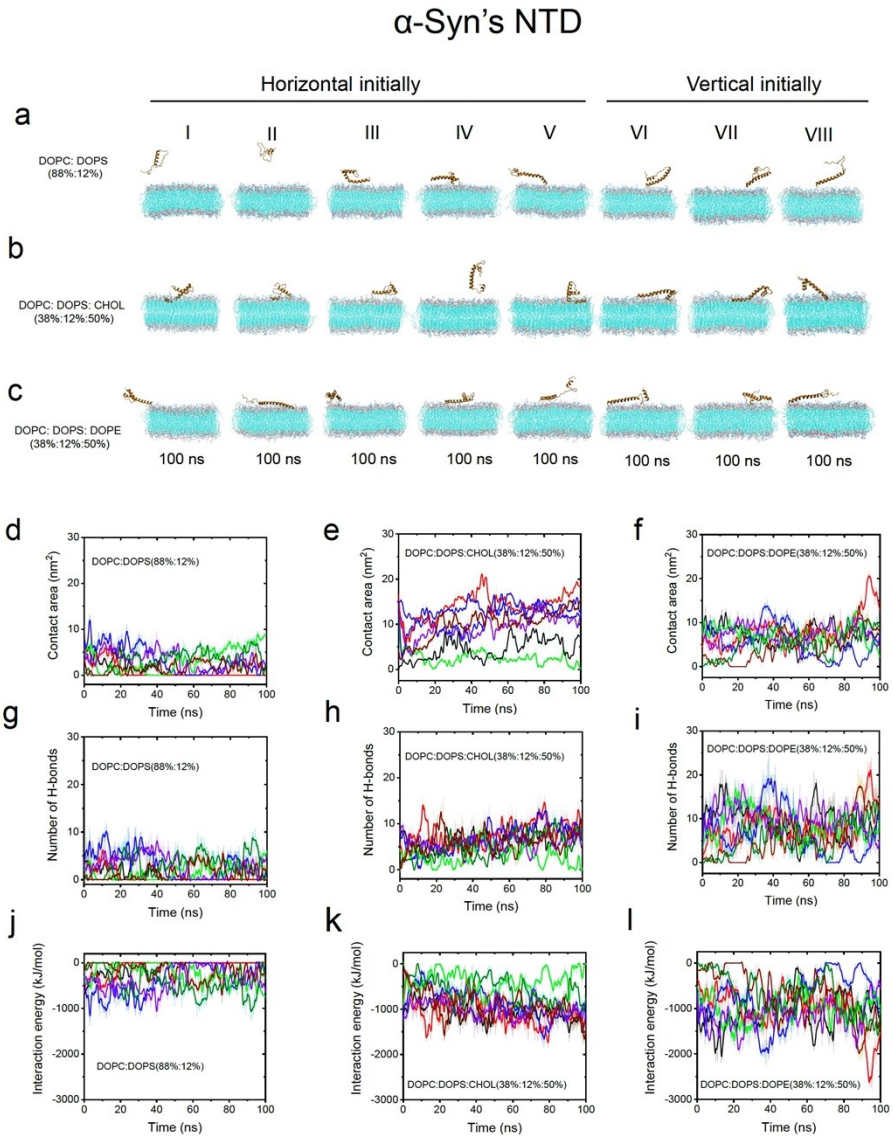

Figure S10. Eight independent simulations of NTD binding to a flat membrane. (a), (b), and (c) Final states of the 100 ns simulations of NTD binding to membranes with varied lipid components. The roman numerals I, II, III, IV, V, VI, VII, and VIII labelled eight independent simulations. (d) to (f), (g) to (i), and (j) to (l) show the contact area, the number of H-bonds, and the interaction energy of corresponding simulations, respectively. Each line in (d) to (l) by individual color represents the result of one of the independent simulations.

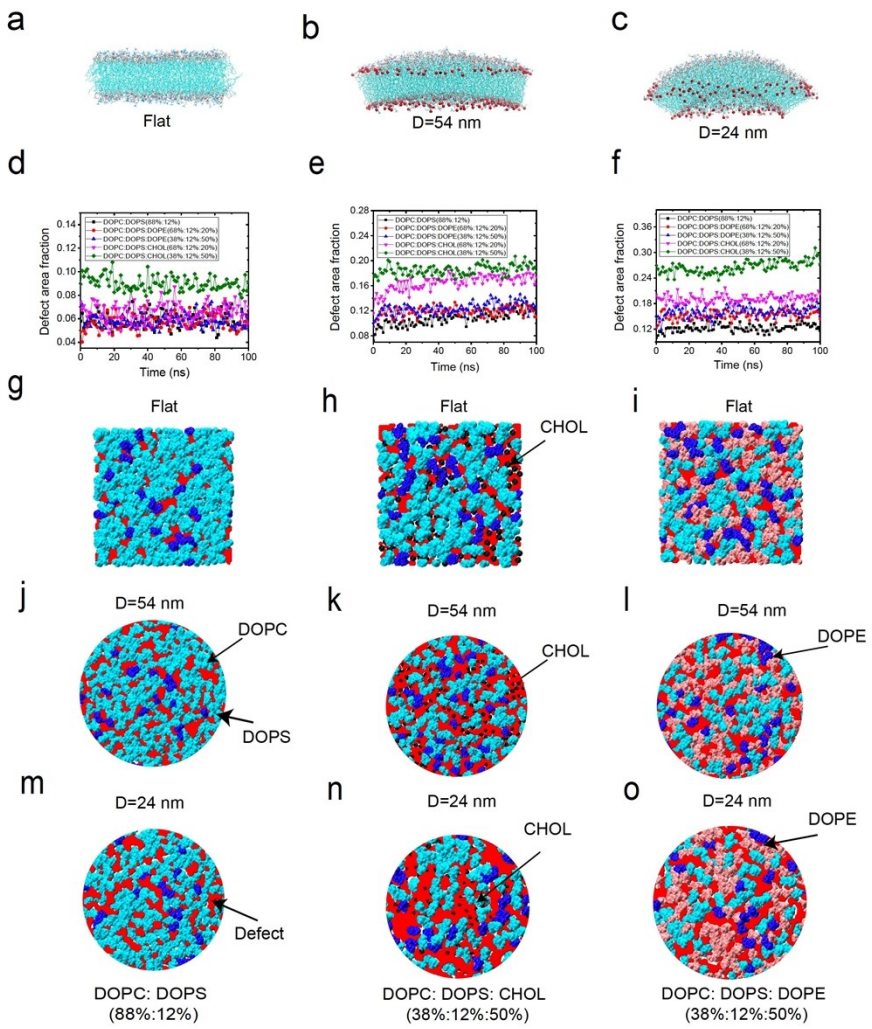

Figure S11. Defect analysis in curved membranes. (a) to (c) Simulated flat and curved membrane models with diameter D = 54 nm and D = 24 nm, respectively. To maintain the curvature of membrane, the lipids' phosphorus atoms at the edge and the inner leaflet of the caps were restrained, as shown by the red dots. (d) to (f) The evolution of the defect area fraction to the total membrane area with flat and curved membranes with D = 54nm and D = 24nm, respectively. In simulations, we tested various lipid components, i.e., the cases of DOPC:DOPS (88%:12%), DOPC:DOPS:DOPE (68%:12%:20%), DOPC:DOPS:DOPE (38%:12%:50%), DOPC:DOPS:CHOL (68%:12%:20%), and DOPC:DOPS:CHOL (38%:12%:50%). (g) to (o) Illustrations of membrane defects with varied curvatures and lipid components. To clarify, defects are illustrated by red region, while the lipids DOPC, DOPS, CHOL, and DOPE are shown by cyan, blue, black, and pink ones, respectively.

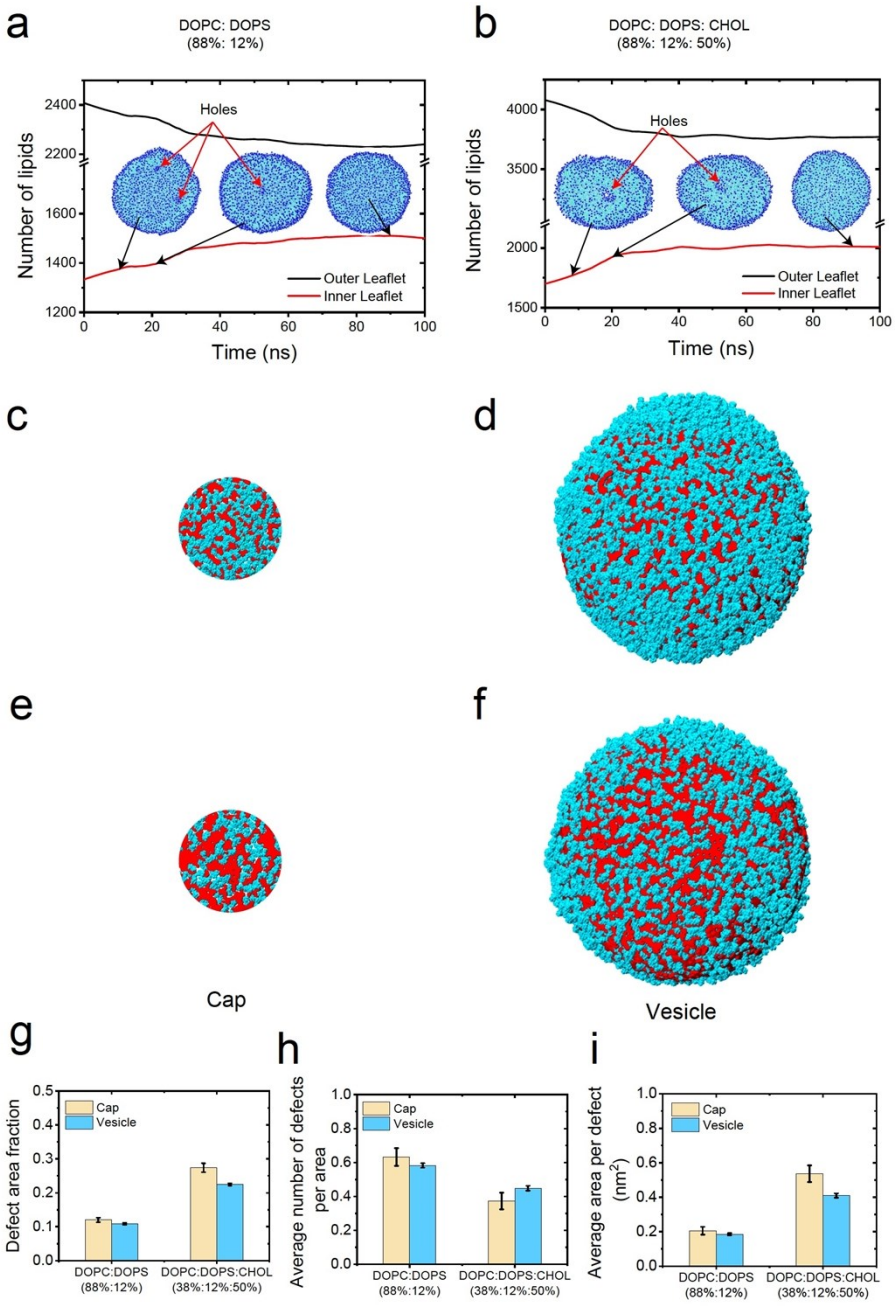

Figure S12. Defect analysis for comparison between cap and vesicle models of a diameter 24 nm. (a) and (b) The number of lipids in the inner and outer leaflet with time in simulations in vesicle containing DOPC:DOPS (88%:12%) and DOPC:DOPS:CHOL (38%:12%:50%), respectively. The insets in (a) and (b) show the structure evolution of the vesicles. Initially there are holes in the vesicles, causing the lipids exchange between the inner and outer leaflet. After about 80 ns simulations all of the holes healed and the number of lipids in the inner and outer leaflet unchanged. (c) and (d) Illustrations of the defects in

the cap and the vesicle models with lipid components DOPC:DOPS (88%:12%), respectively. (e) and (f) Illustrations of the defects in the cap and the vesicle models with lipid components DOPC:DOPS:CHOL (38%:12%:50%), respectively. The defects were represented by red color. (g), (h), and (i) The comparison of the defect area fraction, the average number of defects per area, and the average area per defect in the cap and vesicle models with varied lipid components, respectively. The error bars of the defect area fraction, average number of defects per area, and the average area per defect in the vesicle models are the standard deviations of the results from simulation time 80 ns to 100 ns in each corresponding simulation.

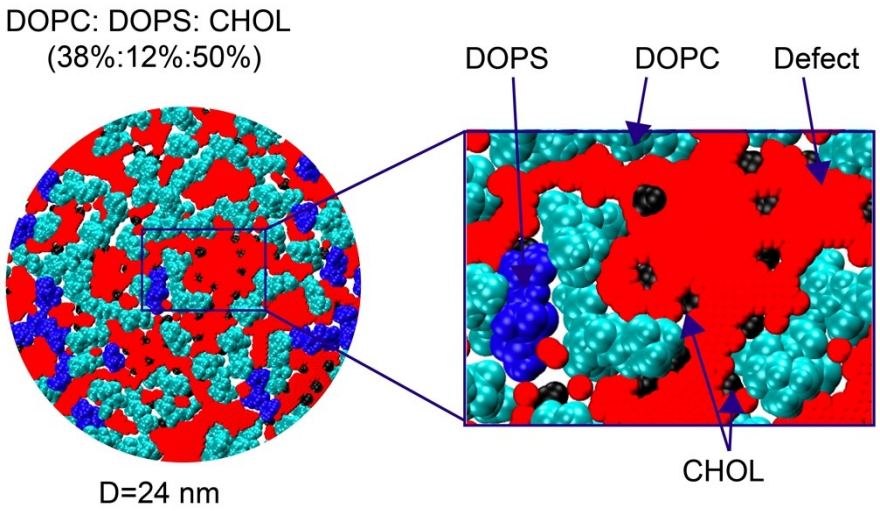

Figure S13. CHOL connects small defect regions to form a large one. The hydrophilic head group of CHOL (-OH) is much smaller than that of other lipids, so that there will be gaps between the CHOL lipids, as well as between the CHOL and other lipids, which expose the hydrophobic tails to form defects. As a result, the enrichment of CHOL may connect some of small defects nearby to become a connected large region that enhances the binding of proteins. The defects are illustrated by red regions, while the lipids DOPC, DOPS, and CHOL by cyan, blue, and black ones, respectively.

References:

1. D. W. Buchan, F. Minneci, T. C. Nugent, K. Bryson and D. T. Jones, *Nucleic Acids Res*, 2013, **41**, W349-357.
2. D. T. Jones, *J Mol Biol*, 1999, **292**, 195-202.
3. T. S. Ulmer, A. Bax, N. B. Cole and R. L. Nussbaum, *J Biol Chem*, 2005, **280**, 9595-9603.
4. S. Jo, T. Kim, V. G. Iyer and W. Im, *J Comput Chem*, 2008, **29**, 1859-1865.
5. K. J. Boyd and E. R. May, *J. Chem. Theory Comput.*, 2018, **14**, 6642-6652.
6. L. Vamparys, R. Gautier, S. Vanni, W. F. D. Bennett, D. P. Tieleman, B. Antonny, C. Etchebest and P. F. J. Fuchs, *Biophys. J.*, 2013, **104**, 585-593.